A Pendulum Driven by a Crank-Shaft-Slider Mechanism and a DC Motor—Mathematical Modeling, Parameter Identification, and Experimental Validation of Bifurcational Dynamics

Grzegorz Wasilewski, Grzegorz Kudra, Jan Awrejcewicz, Maciej Kaźmierczak, Mateusz Tyborowski and Marek Kaźmierczak

Abstract In this work, we investigate numerically and experimentally the dynamics of a pendulum vertically excited by a crank-shaft-slider mechanism driven by a DC motor. The power supplied to the DC is small enough to observe return influence of the pendulum dynamics on the motor angular velocity. In the performed experiments, the motor is supplied with constant time voltages. A series of experimental periodic solutions allowed to estimate the model parameters and, in the further step, predict bifurcation phenomena observed in the real object.

G. Wasilewski · G. Kudra (✉) · J. Awrejcewicz · M. Kaźmierczak · M. Tyborowski · M. Kaźmierczak
Department of Automation, Biomechanics and Mechatronics,
Lodz University of Technology, 1/15 Stefanowski St., 90-924 Łódź, Poland
e-mail: grzegorz.kudra@p.lodz.pl

G. Wasilewski
e-mail: grzegorz.wasilewski@p.lodz.pl

J. Awrejcewicz
e-mail: jan.awrejcewicz@p.lodz.pl

M. Kaźmierczak
e-mail: 182720@edu.p.lodz.pl

M. Tyborowski
e-mail: 82777@edu.p.lodz.pl

M. Kaźmierczak
e-mail: marek.kazmierczak.1@p.lodz.pl

J. Awrejcewicz (ed.), *Dynamical Systems: Theoretical and Experimental Analysis*, Springer Proceedings in Mathematics & Statistics 182, DOI 10.1007/978-3-319-42408-8_31

1 Introduction

There exist a lot of studies on nonlinear dynamics of mechanical systems composed of pendulums in different configurations, including plane or spatial, single or multiple, and sometimes parametrically excited pendulums. Physicians are particularly interested in those kinds of the dynamical systems, since they are relatively simple but can exhibit almost all aspects and phenomena of nonlinear dynamics. In some cases, an experiment is performed in order to confirm analytical or numerical investigations [1–3]. Sometimes, in order to achieve a good agreement between the model's predictions and experimental data, one must take into account many details concerning physical modeling of the real process [3].

When considering behavior of the real dynamical systems, one can encounter a problem of mutual interactions between the oscillatory system and the energy source of limited power, i.e., nonideal energy source. Belato et al. [4] investigated numerically, the electromechanical system composed of a pendulum excited by a crank-shaft-slider mechanism driven by a DC motor considered as a limited power source. A comprehensive numerical analysis of bifurcational dynamics of a similar mechanical system is presented in [5]. An extensive review on the nonideal vibrating systems one can find in [6].

In the work [7], the authors investigated both numerically and experimentally an electromechanical system consisting of a pendulum suspended on the slider of a crank-slider mechanism driven by a DC motor. Since the power of the motor was relatively high, the angular velocity of the shaft was almost constant. Mathematical modeling of the same system under simplifying assumption of a constant angular velocity of the crank, together with the improved algorithm of the parameters' estimation, is presented in [8].

In the present work, the same structure of the mathematical model as in [7] is used in the analysis of the similar real electromechanical system, but in the case of relatively low power supplied to the DC motor, resulting in more variable angular velocity of the crank. This work is also an extended version of the conference publication [9]. In comparison to the work [9], the identification process has been repeated because of small changes in the experimental rig resulting from certain technical reasons. Moreover some additional parameters (previously assumed as known) have been added to the set of identified parameters (for details see Sect. 4). Further bifurcation analysis and model validation in Sect. 5 have also been extended by additional analysis of some irregular attractors and more detailed analysis of the threshold of chaos near the $u_0 = -8.4$ V.

2 Experimental Rig

Figure 1 presents the experimental setup of mathematical model that will be described in next part of the paper. A voltage generator 1 supplies the low-power DC motor 3. Output shaft of the motor is connected with steel shaft 5 by aluminium

coupling 4. Shaft 5 is embedded in pair of ball bearings 6 that provides alignment of shafts. Ball bearings are mounted on 'L' bracket 7a with additional two brackets in 'C' 7b and 'L' 7c shape that support first one to be more stable. Two aluminium strips 7d act as rails to set 'L' bracket both with ball bearings and with DC motor to set them in right position.

There is also the possibility to change low-power DC motor into other one with higher power. On the other end of shaft 5 there is mounted disk 8. Angular position of disk is measured by the use of encoder 9 (type MHK, 360 steps) supplied by wire 10. Rotational motion of disk is transformed thanks to joint 11 (connecting bar) into linear motion of the slider 12 moving on two horizontal guides 13. To the slider there is mounted bracket with two ball bearings 14 (same type as 5) and shaft 15 inserted into them. On this part there is seated physical pendulum 16. In identical way like disk, angular position of pendulum is measured by two types of encoders. 17 is the same type like in case of measuring position of disk. Encoder 18 (type MAB-analog out, supplied by to batteries 19) is used to perform longer measurement, because encoder 17 (type MHK, 3600 steps) have a high resolution what really quickly fills up available space on PC hard disk. All data from encoders are collected by data acquisition devices 2.

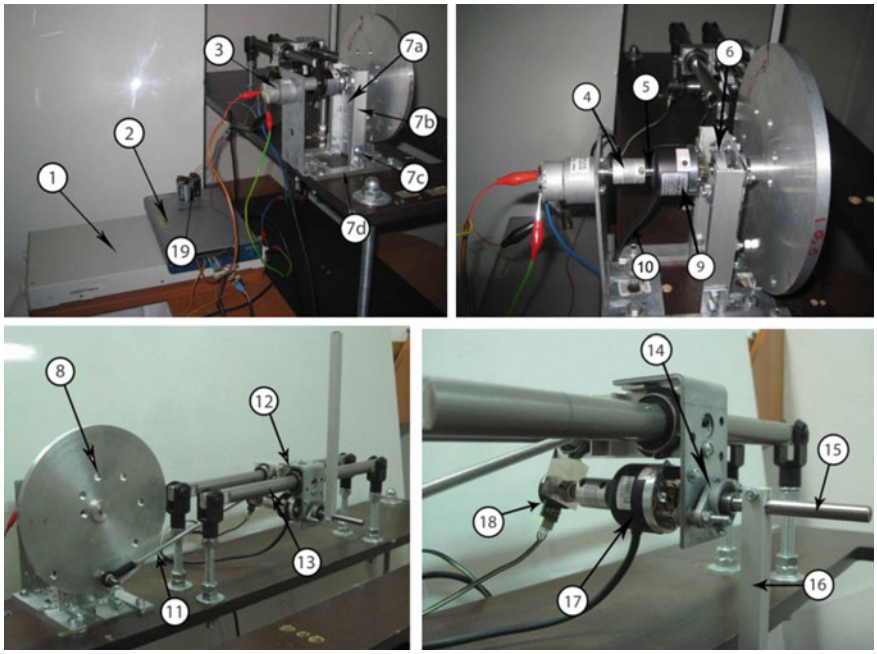

Fig. 1 Experimental setup

3 Mathematical Modeling

In this section, there is presented the mathematical model of the experimental rig presented in Sect. 2. It is based on the results published in the work [7]. Figure 2a exhibits a block diagram presenting the general structure of the system. It is composed of two main subsystems: (i) DC motor (understood as a pure electrical object converting the electrical energy to the mechanical torque; (ii) a two-degree-of-freedom mechanical system including all mechanical elements of the system. The input signal (being under control) is the voltage $u(t)$ supplied to the DC motor. The two coordinates $\theta(t)$ and $\varphi(t)$ determining the position of the mechanical system are assumed to be outputs.

For an armature-controlled DC motor equipped with a gear transmission and assuming that the armature inductance is negligible, one gets the following equation

$$M = \frac{K_T}{R} i_g u - \frac{K_E K_T}{R} i_g^2 \frac{d\theta}{dt}, \tag{1}$$

where M is the torque on the output shaft of the gear transmission, u—input voltage, θ—angular position of the output shaft of the gear transmission, i_g—reduction ratio of the gear transmission, R—armature resistance, K_T—the proportionality constant between the torque generated on the output shaft of the DC motor and the armature current, and K_E—the proportionality constant between the back electromotive force and the angular velocity of the DC motor.

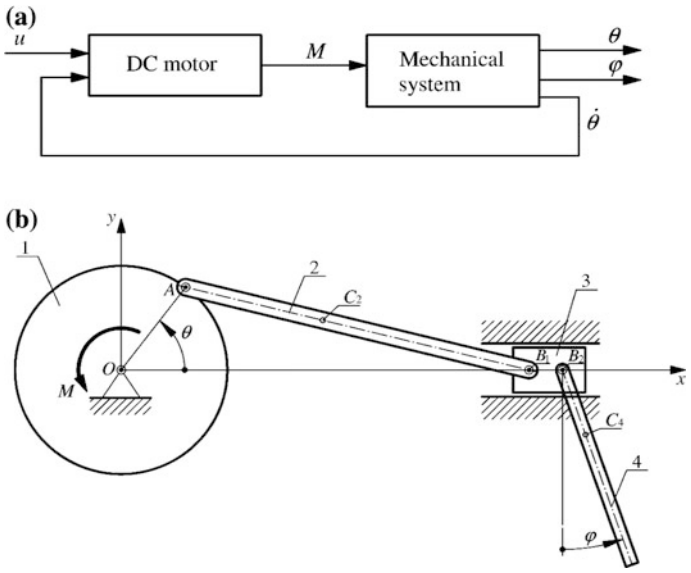

Fig. 2 Physical model of the system

A sketch of a physical model of the mechanical section of the system is depicted in Fig. 2b. This plane two-degree-of-freedom mechanical system is composed of four rigid bodies (1—disk, 2—connecting bar, 3—slider, 4—pendulum) connected by the use of four rotational joints (O, A, B_1, and B_2). Masses of the links 2–4 are denoted as m_b, m_S, and m, respectively. Moments of inertia of the bodies 1, 2, and 4, with respect to their mass centers (located in the points O, C_2, and C_4), are represented by the symbols I_O, I_b, and I, respectively. The corresponding lengths of the mechanical system are denoted as follows: $a = OA$, $b = AB$, $b_1 = AC_2$, and $r = BC_4$. The position of the system is determined by two angles: θ—angular position of the disk (equal to the angular position of the gear transmission output shaft) and φ—angular position of the pendulum. The disk 1 represents all rotating elements of the DC motor, gear transmission, and real disk of the experimental rig.

The governing equations of the investigated system read

$$\mathbf{M}(\mathbf{q})\,\ddot{\mathbf{q}} + \mathbf{N}(\mathbf{q})\dot{\mathbf{q}}^2 + \mathbf{w}(\mathbf{q}) = \mathbf{f}(t) - \mathbf{r}(\mathbf{q},\,\dot{\mathbf{q}}), \tag{2}$$

where

$$\begin{aligned}
\mathbf{q} &= \begin{Bmatrix} \theta \\ \varphi \end{Bmatrix},\ \dot{\mathbf{q}} = \begin{Bmatrix} \dot{\theta} \\ \dot{\varphi} \end{Bmatrix},\ \ddot{\mathbf{q}} = \begin{Bmatrix} \dot{\theta} \\ \ddot{\varphi} \end{Bmatrix},\ \dot{\mathbf{q}}^2 = \begin{Bmatrix} \dot{\theta}^2 \\ \dot{\varphi}^2 \end{Bmatrix}, \\
\mathbf{M}(\mathbf{q}) &= \begin{bmatrix} I_{\mathrm{O}} + a^2\left(F^2(m+m_S) + F_1^2 m_b\right) + \frac{a^2}{b^2}\cos^2\theta\left((b-b_1)^2 m_b + G^2 I_b\right) & -amrF\cos\varphi \\ -amrF\cos\varphi & I + mr^2 \end{bmatrix}, \\
\mathbf{N}(\mathbf{q}) &= = \begin{bmatrix} aFH\left(1+\frac{m_S}{m}\right) + aF_1H_1 - \frac{a^2}{2b^2}\,\mathbf{sin2\theta}\left((b-b_1)^2 m_b + G^2 I_b\left(1 - \frac{a^2}{b^2}G^2\,\mathbf{cos^2\theta}\right)\right) & amrF\,\mathbf{sin\varphi} \\ -rH\,\mathbf{cos\varphi} & 0 \end{bmatrix}, \\
\mathbf{w}(\mathbf{q}) &= \begin{Bmatrix} \frac{a}{b}(b-b_1)m_b g\cos\theta \\ mgr\sin\varphi \end{Bmatrix},\ \mathbf{f}(t) = \begin{Bmatrix} M(t) \\ 0 \end{Bmatrix},\ \mathbf{r}(\mathbf{q},\dot{\mathbf{q}}) = \begin{Bmatrix} M_{R\theta}(\theta,\dot{\theta}) \\ M_{R\varphi}(\dot{\varphi}) \end{Bmatrix},
\end{aligned} \tag{3}$$

and where one has used the following notation

$$G = \frac{1}{\sqrt{1 - \frac{a^2}{b^2}\sin^2\theta}},\ F = \left(1 + \frac{a}{b}G\cos\theta\right)\sin\theta,\ F_1 = \left(1 + \frac{ab_1}{b^2}G\cos\theta\right)\sin\theta,$$

$$H = am\left(\cos\theta + \frac{a}{b}G\cos 2\theta + \frac{1}{4}\frac{a^3}{b^3}G^3\sin^2 2\theta\right),$$

$$H_1 = am_b\left(\cos\theta + \frac{ab_1}{b^2}G\cos 2\theta + \frac{1}{4}\frac{a^3 b_1}{b^4}G^3\sin^2 2\theta\right). \tag{4}$$

The vector $\mathbf{r}(\mathbf{q}, \dot{\mathbf{q}})$ contains all resistance forces and their components

$$M_{R\theta}(\theta, \dot{\theta}) = c_O\dot{\theta} + \frac{2}{\pi}M_O \arctan(\varepsilon_O\dot{\theta}) + a^2F^2c_S\dot{\theta} - \frac{2}{\pi}aFT_S \arctan(-\varepsilon_S aF\dot{\theta}),$$

$$M_{R\varphi}(\dot{\varphi}) = c_B\dot{\varphi} + \frac{2}{\pi}M_B \arctan(\varepsilon_B\dot{\varphi}), \tag{5}$$

The terms $c_O\dot{\theta}$ and $\frac{2}{\pi}M_O \arctan(\varepsilon_O\dot{\theta})$ represent the viscous damping and dry friction components of the resistance in the joint O, where c_O is viscous damping coefficient, M_O—magnitude of dry friction torque. One assumes that M_O is a constant parameter, independent from the loading of the joint O. The expressions $a^2F^2c_S\dot{\theta}$ and $-\frac{2}{\pi}aFT_S \arctan(-\varepsilon_S aF\dot{\theta})$ represent the viscous damping and dry friction components of resistance between the slider and guide, reduced to the coordinate θ, where c_S and T_S are the corresponding constant parameters. Similarly, the terms $c_B\dot{\varphi}$ and $\frac{2}{\pi}M_B \arctan(\varepsilon_B\dot{\varphi})$ are viscous damping and dry friction components in the joint B_2. The quantities ε_O, ε_S and ε_B are numerical parameters used in the dry friction model regularization. Usually they are relatively large since one wants to approximate accurately the sign function. However it occurs that sometimes the smaller values of these parameters lead to the better results (in the sense of fitting of the simulation results to the experimental data)—one can find an example in the work [8]. In comparison to the work [9], we assume three different parameters ε_O, ε_S, and ε_B (previously they were substituted by one parameter ε). Resistances in the joints A and B_1 are not taken into account.

Finally one gathers the right-hand side of Eq. (6) into one vector

$$\mathbf{f}_r(t, \mathbf{q}, \dot{\mathbf{q}}) = \mathbf{f}(t) - (\mathbf{q}, \dot{\mathbf{q}}) = \\ = \left\{ \begin{array}{c} K_M u(t) - C_O\dot{\theta} - \frac{2}{\pi}M_O \arctan(\varepsilon_O\dot{\theta}) - a^2F^2c_S\dot{\theta} + \frac{2}{\pi}aFT_S \arctan(-\varepsilon_S aF\dot{\theta}) \\ -c_B\dot{\varphi} - \frac{2}{\pi}M_B \arctan(\varepsilon_B\dot{\varphi}) \end{array} \right\}, \tag{6}$$

where

$$K_M = \frac{K_T}{R}i_g,\ C_O = \frac{K_E K_T}{R}i_g^2 + c_O.$$

Let us note, that the mechanical viscous damping in the joint O and the back electromotive force (multiplied by some other constants) have mathematically the same influence on the final torque on the output shaft of the gear transmission. They are mathematically indistinguishable and unidentifiable in the developed model. Their aggregate action is defined by the coefficient C_O.

4 Parameter Estimation

In the process of identification, one has used three experimental solutions, with the input signal $u(t)$ in a form of step function with zero initial value, and constant final value u0, equal to −10.8, −8.0 and −6.5 V, respectively. The initial conditions are the same for all experiments: $\theta(0) = -\frac{\pi}{2}$ rad, $\varphi(0) = 0$ rad, $\dot{\theta}(0) = 0$ rad/s, and $\dot{\varphi}(0) = 0$ rad/s. The solutions tend to periodic attractors, which allows to avoid problems of identification related to high sensitivity to initial conditions. The angles $\varphi(t)$ and $\theta(t)$ were recorded on the time interval [0, 60] s.

Because of nonideal behavior of resistances in the system (small random fluctuations of friction), the angular velocity of the disk undergoes some random changes, which cannot be described by the use of deterministic equations. These changes are not big, but after some time they can lead to significant time shift in the angular position of the disk. It may cause problems in fitting of the simulated signals to those obtained experimentally, if we express them in the time domain. This is the reason of the idea to compare the corresponding signals expressed as functions of angular position of the disk θ.

Since we plan to use in the estimation process two different signals (angular position of the pendulum and angular velocity of the disk), we construct the objective function F_o in the form of weighted sum of two different parts

$$F_O(\boldsymbol{\mu}) = w_\varphi F_{O\varphi}(\boldsymbol{\mu}) + w_\omega F_{O\omega}(\boldsymbol{\mu}), \tag{7}$$

where $\boldsymbol{\mu}$ is vector of the estimated parameters, w_φ and w_ω are the corresponding weights, and where

$$F_{O\varphi}(\boldsymbol{\mu}) = \frac{1}{\sum_{i=1}^{N} \left(\theta_{fi} - \theta_0\right)} \sum_{i=1}^{N} \int_{\theta_0}^{\theta_{fi}} \left(\varphi_{si}(\theta, \boldsymbol{\mu}) - \varphi_{ei}(\theta, \boldsymbol{\mu})\right)^2 d\theta,$$

$$F_{O\omega}(\boldsymbol{\mu}) = \frac{1}{\sum_{i=1}^{N} \left(\theta_{fi} - \theta_0\right)} \sum_{i=1}^{N} \int_{\theta_0}^{\theta_{fi}} \left(\omega_{fsi}(\theta, \boldsymbol{\mu}) - \omega_{fei}(\theta, \boldsymbol{\mu})\right)^2 d\theta. \tag{8}$$

In the expressions (8) N denotes number of the compared pairs of solutions, θ_0 is common initial angle θ, θ_{fi} ($i = 1, 2, \ldots, N$) are final angular positions of the disk, φ_{si} and φ_{ei} are angular positions of the pendulum obtained by the use of i-th numerical simulation and experiment, correspondingly. Since we measure the angular position of the disk, we differentiate this signal with respect to time in order to obtain the corresponding angular velocity. We do it numerically, by passing the signal $\theta_{ei}(t)$ (obtained by the linear interpolation of the experimental data) through the filter of the transfer function $G_f(s) = \frac{s}{\left(T_f s + 1\right)^2}$. As an output we obtain the signal $\omega_{fei}(t)$, which appears in the expressions (8), but as a function of the angle θ. In

order to have the proper simulation signal, which could be compared with the signal ω_{fei}, we also pass through the filter $G_f(s)$ the numerical signal $\theta_{si}(t)$, obtaining $\omega_{fsi}(t)$.

Using the functions (8), one assumes that initial conditions and input signals $u(t)$ are known and they are the same for both the experiment and simulation. Moreover, some parameters' values are easy to obtain by the direct measurements of masses and lengths. They are assumed to be constant during the identification process: $m_b = 0.057\,\text{kg}$, $m_S = 0.777\,\text{kg}$, $m = 0.226\,\text{kg}$, $a = 0.080\,\text{m}$, and $b = 0.300\,\text{m}$. Other parameters assumed to be constant are: $\varepsilon_O = 10^3$, $g = 9.81\,\text{m}\,\text{s}^{-2}$. The remaining parameters (as the elements of the vector $\boldsymbol{\mu}$) will be obtained by minimization of the objective function F_o, using the Nelder–Mead method [10, 11], also known as downhill simplex method. This is commonly used optimization algorithm, implemented in MATLAB and Scilab functions *fminsearch*. One also assumes the following values of the weights and the time constant of the filter: $w_\varphi = 1\,\text{rad}^{-2}$, $w_\omega = 1\,\text{s}^2\,\text{rad}^{-2}$, and $T_f = 0.1\,\text{s}$.

In the estimation process one obtained the following values of the model parameters: $K_M = 3.066 \times 10^{-2}\,\text{N m/V}$, $C_O = 3.003 \times 10^{-2}\,\text{N m s}$, $M_O = 1.937 \times 10^{-2}\,\text{N m}$, $I_O = 5.252 \times 10^{-3}\,\text{kg m}^2$, $I_b = 2.373 \times 10^{-6}\,\text{kg m}^2$, $b_1 = 8.801 \times 10^{-2}\,\text{m}$, $c_S = 2.171 \times 10^{-1}\,\text{N s}$, $T_s = 6.583 \times 10^{-1}\,\text{N}$, $I = 1.426 \times 10^{-3}\,\text{kg m}^2$, $r = 5.417 \times 10^{-2}\,\text{m}$, $c_B = 2.486 \times 10^{-4}\,\text{N m s}$, $M_B = 2.162 \times 10^{-3}\,\text{N m}$, $\varepsilon_S = 27.68$ and $\varepsilon_B = 3.193$. Figure 3 exhibits comparison of four numerical solutions $\varphi(\theta)$ to the model with the corresponding experimental data used during the identification process (only the final parts of the solutions are presented). In Fig. 4, there are presented the comparison of the corresponding solutions $\omega_f(\theta)$. The optimal value of the objective function (7) is 2.298×10^{-3}. Note that in comparison to the work [9] the parameters ε_S and ε_B have been added to the set of the identified parameters, which allow to obtain better modeling results (see the comments in Sect. 1 and the work [8]).

5 Bifurcation Dynamics

Further experimental investigations of the systems showed that it can also exhibit irregular behavior. For example the constant input voltage of −8.51 V leads to irregular dynamics, with full rotations of the pendulum, presented in Fig. 5. These solutions were not used in the identification process because of potential problems related to high sensitivity to initial conditions. However, they are confirmed qualitatively very well by the developed mathematical model and its numerical simulations, as shown in Fig. 5.

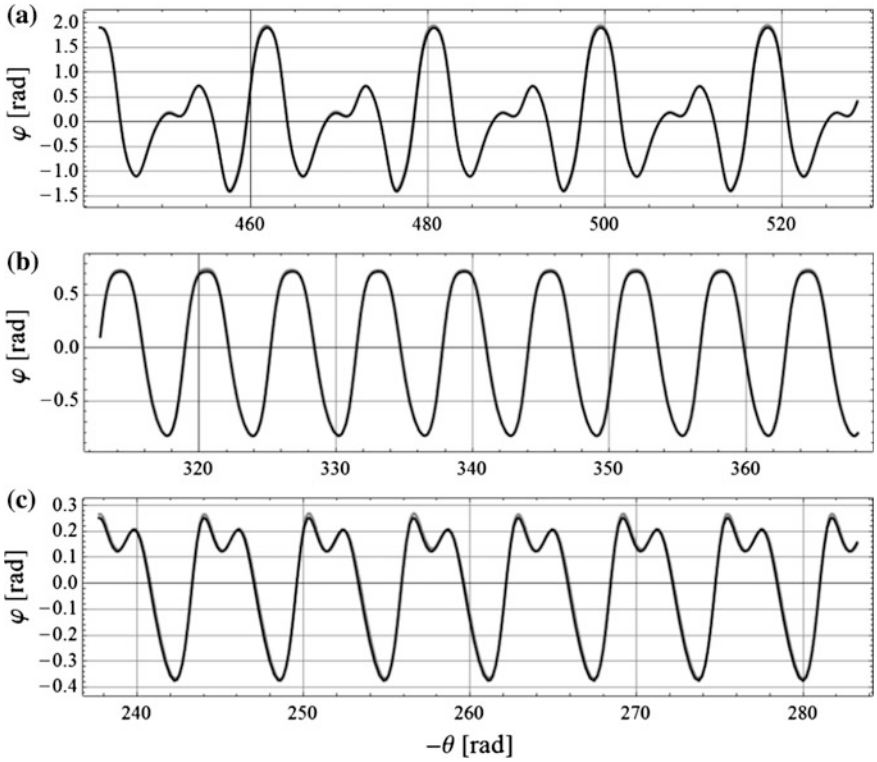

Fig. 3 Three numerical solutions $\varphi(\theta)$ (*black line*) compared with the corresponding experimental data (*gray line*) ($u_0 = -10.8$, -8.0, and -6.5 V, for subfigures **a**, **b**, and **c**, respectively)

In Fig. 6, there are presented the Poincaré sections of exemplary irregular attractors (they are constructed by sampling of the system state at the instances, when the angular position $\theta(t)$ of the disk crosses the zero position) exhibited by mathematical model for $u_0 = -11.3$ V (a), -10.3 V (b), -9.01 V (c), and -8.51 V (d). The examples (a–b) correspond to quasiperiodic behavior of the system, while the sections (c–d) indicate the chaotic character of the attractor. Figure 7 exhibits bifurcation diagrams of the mathematical model—for quasi-statically changing the bifurcation parameter u_0 from -13 to -5 V (a) and from -5 to -13 V (b), confirming the chaotic window around the value $u_0 = -8.51$ V and many other zones of interesting bifurcational dynamics. In Fig. 8 one can observe results of numerical (a) and experimental (b) investigations of the threshold of the chaotic behavior of the system (for decreasing control parameter) near the $u_0 = -8.4$ V seen in Fig. 7. In the experimental investigations, the control parameter has been changed from -8.3 V to -8.48 with the speed of -0.0015 V/s (the investigation lasted 120 s).

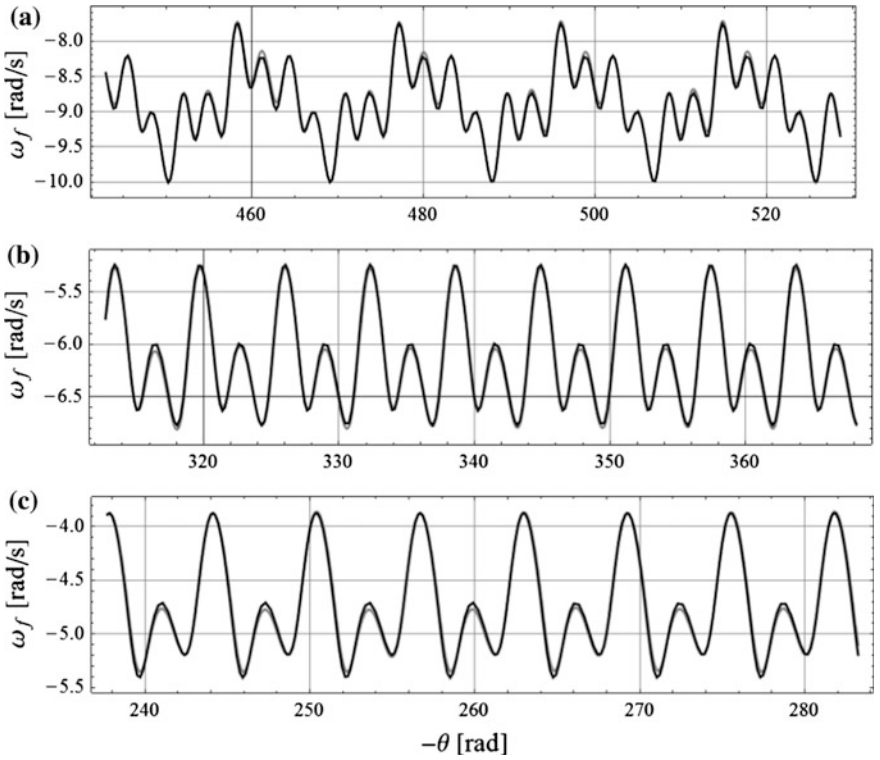

Fig. 4 Three numerical solutions $\omega_f(\theta)$ (*black line*) compared with the corresponding experimental data (*gray line*) ($u_0 = -10.8$, -8.0, and -6.5 V, for subfigures **a**, **b** and **c**, respectively)

Then the same condition was reconstructed during numerical simulations. One can notice 0.05 V of difference between the borders of the chaotic window observed numerically and experimentally.

6 Concluding Remarks

In the paper, there have been presented the results of the preliminary phase of the larger project aimed in numerical and experimental analysis of different configurations of a pendulum driven by an electric motor. In the current stage, one developed a mathematical and simulation model of real physical object being a physical pendulum excited vertically by a crank-shaft-slider mechanism, which is driven by a DC motor.

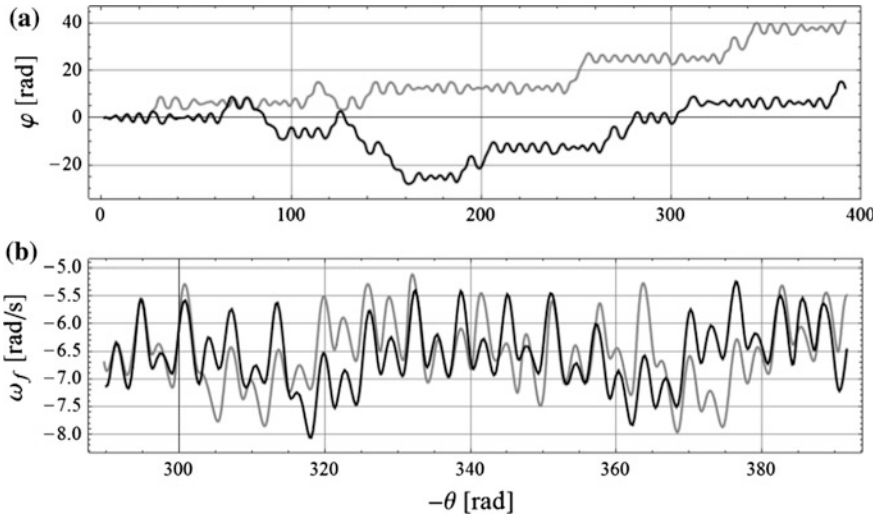

Fig. 5 The chaotic numerical solutions (*black lines*) $\varphi(\theta)$ (**a**) and $\omega_f(\theta)$ (**b**) compared with the corresponding experimental data (*gray lines*) for $u_0 = -8.51$ V

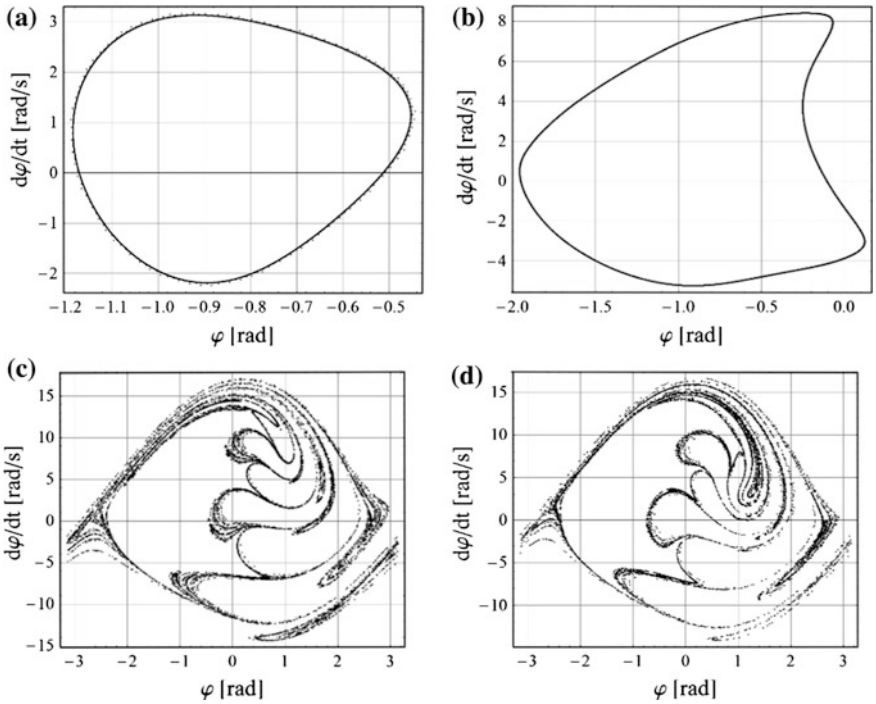

Fig. 6 Poincaré sections of the attractors obtained numerically for $u_0 = -11.3$ V (**a**), -10.3 V (**b**), -9.01 V (**c**), and -8.51 V (**d**)

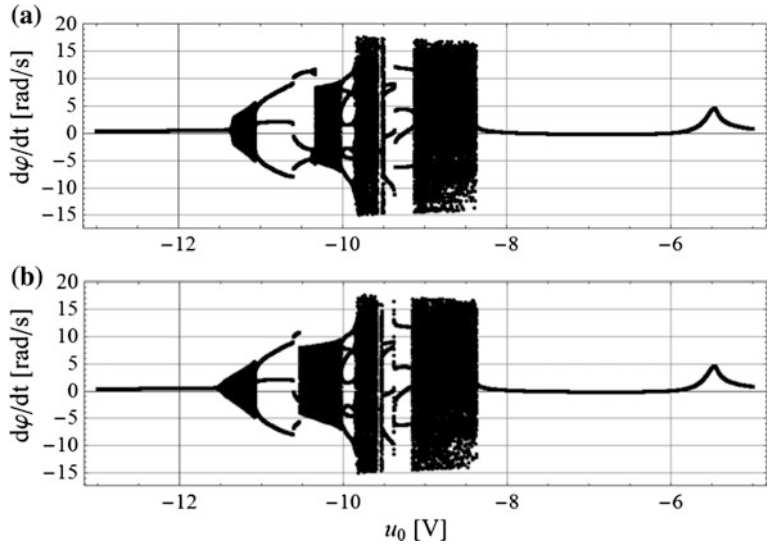

Fig. 7 Bifurcation diagram with constant in time input voltage u_0 as a control parameter—for growing (**a**) and decreasing (**b**) bifurcation parameter

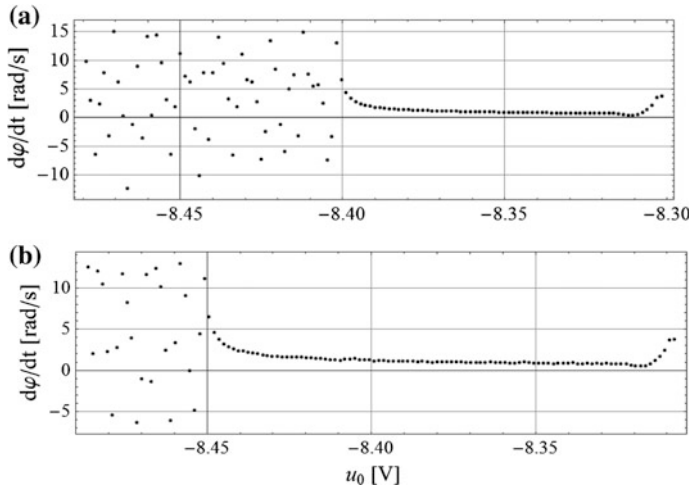

Fig. 8 Numerical (**a**) and experimental (**b**) investigations of the threshold of the chaotic behavior of the system (for decreasing control parameter)

Since the initial goal of the project is to develop exact and reliable mathematical and simulation model of the system, we take into account many details of friction and damping. We have also treated the parameters controlling the functions approximating the sign functions in the dry friction model as the parameters to be

identified from the experimental data. It resulted in a new resistance model rather than in a smooth approximation of the sign function. But this new model leads to better simulation results both in the sense of accuracy and speed of simulation. The second aspect results from the avoidance of stiffness of the differential equation of motion typical for smooth approximation of the sign function.

It should be noted that the a priori knowledge about the system was very poor including the knowledge about the DC motor and the gear transmission. But only three experimental periodic solutions were sufficient for developing a mathematical model mapping the dynamics of real system very well and allowing for reliable numerical simulations.

Acknowledgments The work has been supported by the Polish National Science Centre, MAESTRO 2, No. 2012/04/A/ST8/00738.

This is an extended version of the work [9] presented at the 13th Conference on Dynamical Systems—Theory and Applications, December 7–10, 2015, Łódź, Poland.

References

1. Blackburn, J.A., Zhou-Jing, Y., Vik, S., Smith, H.J.T., and Nerenberg, M.A.H. Experimental study of chaos in a driven pendulum. *Physica D* 26, 1–3 (1987), pp. 385–395.
2. Zhu, Q., and Ishitobi, M. Experimental study of chaos in a driven triple pendulum. *Journal of Sound and Vibration*, 227, 1 (1999), pp. 230–238.
3. Awrejcewicz, J., Supeł, B., Kudra, G., Wasilewski, G., and Olejnik, P. Numerical and experimental study of regular and chaotic motion of triple physical pendulum. *International Journal of Bifurcation and Chaos* 18, 10 (2008), pp. 2883–2915.
4. Belato, D., Weber, H.I., Balthazar, J.M., and Mook, D.T. Chaotic vibrations of a nonideal electro-mechanical system. *International Journal of Solids and Structures*, 38 (2001), pp. 1699–1706.
5. Avanço, R.H., Navarro, H.A., Brasil, R.M.L.R.F., and Balthazar, J.M. Nonlinear Dynamics of a Pendulum Excited by a Crank-Shaft-Slider Mechanism, *ASME 2014 International Mechanical Engineering Congress and Exposition*, *Volume 4B: Dynamics, Vibration, and Control*, Montreal, Quebec, Canada, 2014.
6. Cveticanin, L. Dynamics of the non-ideal mechanical systems: A review. *Journal of the Serbian Society for Computational Mechanics* 4, 2 (2010), pp. 75–86.
7. Kaźmierczak, M., Kudra, G., Awrejcewicz, J., and Wasilewski, G. Numerical and experimental investigation of bifurcational dynamics of an electromechanical system consisting of a physical pendulum and DC motor, in: Awrejcewicz J., Kaźmierczak M., Olejnik P. and Mrozowski J. (eds.) *Dynamical Systems – Applications.* TU of Lodz Press, Lodz, 2013, pp. 49–58.
8. Kaźmierczak, M., Kudra, G., Awrejcewicz, J., and Wasilewski, G. Mathematical modelling, numerical simulations and experimental verification of bifurcation dynamics of a pendulum driven by a dc motor. *European Journal of Physics* 36, 5 (2015), 13 pages.
9. Wasilewski G., Kudra G., Awrejcewicz J., Kaźmierczak M., Tyborowski M., and Kaźmierczak M. Experimental and numerical investigations of a pendulum driven by a low-powered DC motor, in: Awrejcewicz J., Kaźmierczak M., Olejnik P. and Mrozowski J. (eds.) *Dynamical Systems—Mathematical and Numerical Approaches*, TU of Lodz, Lodz, 2015, pp. 579–590.

10. Gershenfeld, N. *The Nature of Mathematical Modelling*. Cambridge University Press, 2011.
11. Nelder, J.A., and Mead, R. A simplex method for function minimization. Computer Journal 7, 4 (1965), pp. 308–313.